JOINT INSTITUTE FOR NUCLEAR RESEARCH
Frank Laboratory and Neutron Physics (FLNP)

# FINAL REPORT ON THE START PROGRAMME

## *A Methylene Blue-Doped Polystyrene Defect Layer in a 1D Photonic Crystal for Gamma Radiation Sensing*

**Supervisor:**
Dr. Zaky. A. Zaky

**Student:**
Mai Medhat El Sayed, Egypt
Beni-Suef University

**Participation period:**
August 17 – September 27,
Summer Session 2025

Dubna, 2025

**Abstract**

We theoretically investigate a 1D photonic crystal detector's response to gamma radiation using a polymer material in the visible spectrum. The proposed photonic crystal (PC) features a defect layer consisting of polystyrene (PS) doped with methylene blue (MB) dye, which exhibits a resonant peak in reflectivity highly sensitive to gamma radiation doses. The PC unit cell consists of alternating layers of silicon dioxide and silicon, analyzed using the characteristic matrix method. We investigate the effects of gamma radiation doses (1000 Rad and 2000 Rad) on resonance and optimize geometrical parameters to enhance sensitivity, quality factor, and spectral characteristics. Our results show that parameters like angle of incidence and layer thickness influence the spectral characteristics of the resonance. With a high sensitivity of 0.029017 nm/Rad and a quality factor of 171.5592, the detector shows promise for optical applications, particularly in radio medical sensing where precise radiation detection is crucial.

## 1. Introduction

Space is permeated by a complex mix of radiation, comprising protons, electrons, neutrons, gamma rays, and high-energy particles, which presents substantial challenges for device development and research. The fabrication of radiation-hardened devices and advanced radiation detection systems are critical areas of focus. Given the high energy and penetrative capabilities of gamma radiation, a detailed grasp of material behavior under gamma irradiation is essential for the advancement of radiation-sensing technologies[1, 2]. Therefore, ionizing radiations, such as gamma rays and electron beams, are crucial for modifying various industrial polymers, including thermoplastics like low and high density of polyethylene LDPE, HDPE, Nylon-6, and Nylon-66, as well as elastomers like silicone elastomer, and ethylene-vinyl acetate EVA copolymer[3-5].

In recent years, polymer materials have garnered significant attention in research due to their intriguing responses to radiation exposure, especially gamma irradiation [6-11]. Polymers are popular due to their low weight, cost-effectiveness, ease of processing, and versatility in producing various sample thicknesses[12]. Research in polymer science continually uncovers new insights, which are gradually being integrated into comprehensive theories about the interrelationships between polymer structure, physical properties, and functional behavior. The concepts of thermodynamics, kinetics, and polymer chain structure synergize to advance the field of polymer science. Irradiation of polymers disrupts their initial structure through mechanisms such as cross-linking, free radical formation, and irreversible bond cleavages, leading to molecular fragmentation and the formation of saturated and unsaturated groups. These processes introduce defects within the material, altering its optical, electrical, mechanical, and chemical properties. In this context, Irradiated polymers are gaining traction for high-performance applications due to their enhanced properties and advantages. Additionally, by incorporating these polymers into photonic crystals (PCs), they can play a vital role in sensing gamma radiation.

Moreover, researchers and scientists have turned to optical sensors based on photonic crystals (PCs), which show promise for detecting and monitoring various chemical, biological, and biomedical substances [13, 14]. To clarify these PCs, are artificial structures that control light propagation through periodic refractive indices [15]. They consist of dielectric materials with alternating refractive indices, creating photonic band gaps (PBGs) that confine and transmit

specific light frequencies [16, 17]. The unique properties of PCs make them attractive for various applications [18, 19]. The construction of PCs often relies on materials with superior optical properties, including semiconductors, metals, superconductors, metamaterials, and liquid crystals[20-23]. PCs are also found in nature, occurring in structures like opal gemstones, beetles, bird feathers, and butterfly wings, as illustrated in fig.1(a, b, c, d). These exhibits striking iridescent colors due to their periodic nanostructures. In this context, PCs can be structured in one, two, or three dimensions as in fig.1(e). Thus, the simplest one from fabrication side and costing effective, it will be in one dimensional PCs.

According to previous literature, there are methods to create PCs, including holographic lithography, layer-by-layer stacking, electrochemical etching, and chemical vapor deposition[24-26].

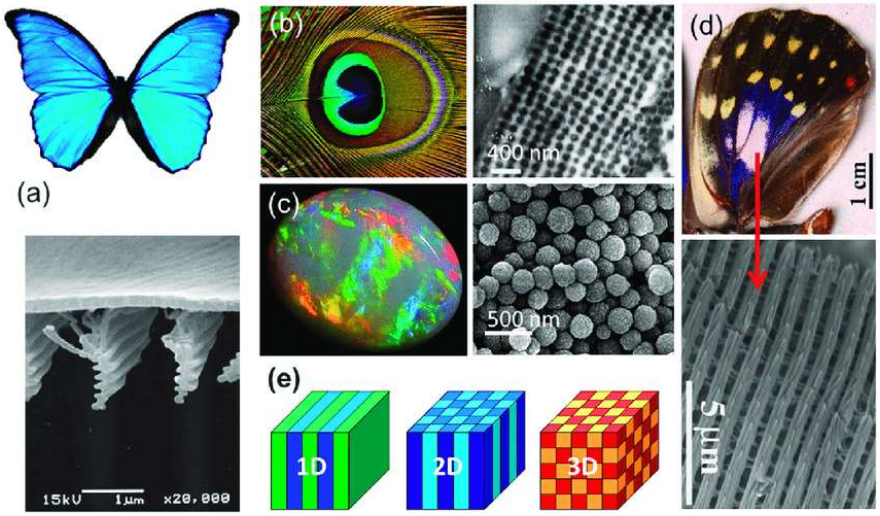


Fig.1: (a, b, c, d) are natural structures of PCs in opals, beetles, bird feathers, and butterfly wings. (e) Simulated PCs through fabrication in 1D, 2D, and 3D [27, 28]

In this regard, PBGs are regions where specific electromagnetic waves EMW frequencies are confined due to Bragg scattering [29, 30]. These PBGs are like electronic band gaps, inhibiting radiation propagation within specific frequency ranges[31, 32]. Therefore, PBGs can trap and guide light through cavities and waveguides. Defect modes can emerge in PBGs when periodicity is disrupted. The characteristics of PBGs are influenced by material properties and structural parameters, enabling photonic crystals to be used in sensors and reflectors for various applications. In 1D photonic crystals, this leads to light localization and resonant peaks. Both PBGs and defect modes can be tuned by external factors like pressure[33, 34] and temperature[35]. This property makes PCs promising for various sensors, including temperature, gas, liquid, and biochemical sensors, as well as biomedical applications like cancer cell detection and glucose monitoring[36-40].

Here, this study investigates how polymer materials respond to varying doses of gamma radiation. Our findings highlight the impact of gamma irradiation on the optical properties of photonic crystals (PCs) based on polystyrene (PS) layers doped with methylene blue (MB) dye. The results suggest that PS films infused with this dye could serve as effective dosimeters integrated into PCs.

## 2. Setup Modeling and Materials

In this section, we introduce a schematic diagram of the designed 1D PCs for detecting gamma radiation surrounded by air and substrate. Here, the PCs layers composed of silicon dioxide SiO2 and silicon Si in one unit cell with periodicity numbers of N and s. Meanwhile, PCs are specified with refractive indices $n_1, n_2$and thickness $d_1$, $d_2$. In this context, we utilize polymer material as a defect layer embedded into PCs. This defect layer is characterized by refractive index $n_D$ and thickness $d_D$. Therefore, we present the configuration of our design on $[(Sio2/Si)^N/ Ps /(SiO2/Si)^s]$. Moreover, we use polystyrene polymer medium through the PCs design as a defect layer. Polystyrene is a hard, rigid, and transparent thermoplastic material at room temperature. It softens and distorts when exposed to heat and is soluble in solvents like aromatic hydrocarbons, cyclohexane, and chlorinated hydrocarbons[41]. Therefore, we employ PCs based on polystyrene (PS) layers doped with methylene blue (MB) dye, used as a solvent in 1D periodic structure, as shown in Fig.2.Additionally, Polystyrene films have been successfully deposited on substrates like glass and silicon wafers by various researchers[42, 43]. In this regard, Al-Ramadhann investigated the impact of gamma radiation on the optical properties of polystyrene thin films doped with anthraquinone copolymer[41].

In beginning, the samples were initially irradiated with a **$^{60}$Co** source, placed at the chamber's center for radiation equilibrium, and exposed to doses between 1000-2000 Rad at room temperature. Additionally, the structure's initial conditions were set for normal light incidence, with layer thicknesses of d1 = 20 nm, d2 = 85.51 nm, and dD = 20 nm, respectively. Then, the outcoming reflectivity(R) and transmittance (T) spectra were measured using spectrophotometer over a wavelength range of 300-600 nm from Visible region.

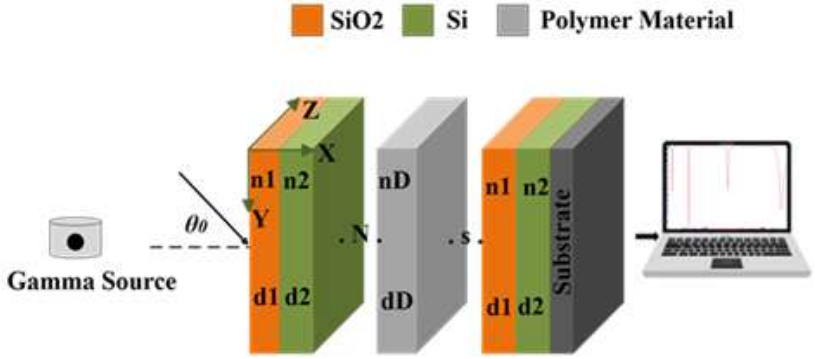


Fig.2: An illustration of the simulation setup for the detection of gamma doses through photonic crystal structure based on defect layer of polystyrene blue which configuration of $[(SiO2/Si)^N/Ps/(SiO2/Si)^s]$ with periodicity numbers of N and s.

## 3. Theoretical Analysis and Methodology

Now, we will outline how incident EMWs interact with our 1D photonic crystal structure. By combining the optical properties of the materials with the transfer matrix method (TMM), we can effectively describe this interaction. Given the structure's periodicity along the X-axis and assuming normal incidence, TMM represents the wave response through each layer in matrix form, enabling us to express the electric and magnetic field components within the unit cell as follows:

$$E_i = A_i \exp(-ik_i x) + B_i \exp(ik_i\, x) \;= E_{x^+} + E_{x^-}$$
$$H_i = \frac{\partial E_i}{i\omega\, \partial x} = \frac{k_i}{\omega}[-A_i \exp(-ik_i x) - B_i \exp\,(ik_i x)] = q_i\,(E_{x^+} - E_{x^-}) \quad (1)$$

Here, $A_i$ and $B_i$ are the field amplitudes in layer $i$, $\lambda$ is the incident wavelength , $k_i$ is the wave vector in layer $i$, and it is formed as $k_i = k_0 n_i cos\theta_i = (2\pi/\lambda)\, n_i\, cos\theta_i$,where $\theta_i$ and $n_i$ are the incidence angle and the refractive index through this layer, respectively. In other formulism, the previous equation could be reformulated as [44, 45] :

$$\begin{pmatrix} E_i \\ H_i \end{pmatrix} = \begin{pmatrix} 1 & 1 \\ q_i & -q_i \end{pmatrix} \begin{pmatrix} E_{x^+} \\ E_{x^-} \end{pmatrix} \quad (2)$$

For a layer $i$ with thickness $d_i = x_1 - x_0$, the electromagnetic wave response between boundaries $x_0$ and $x_1$ takes the following form:

$$\begin{pmatrix} E_0 \\ H_0 \end{pmatrix} = \begin{pmatrix} 1 & 1 \\ q_i & -q_i \end{pmatrix} \begin{pmatrix} \exp[i\, k_i d_i] & 0 \\ 0 & \exp[i\, k_i d_i] \end{pmatrix} \begin{pmatrix} E_{x^1+} \\ E_{x^1-} \end{pmatrix}$$
$$= \begin{pmatrix} \cos(k_i d_i) & (-i/q_i)\sin(k_i d_i) \\ -iq_i \sin(k_i d_i) & \cos(k_i d_i) \end{pmatrix} \begin{pmatrix} E_1 \\ H_1 \end{pmatrix} = w_i \begin{pmatrix} E_1 \\ H_1 \end{pmatrix} \quad (3)$$

The matrix $w_i$ is used to describe the response of incident waves through each layer of the structure along the X-axis, where [45] :

$$w_i = \begin{pmatrix} \cos(q_i) & (-i/\varsigma_i)\sin(q_i) \\ -i\varsigma_i \sin(q_i) & \cos(q_i) \end{pmatrix} \quad (4)$$

For TM polarization, the components $q_i$ and $\varsigma_i$ equal $\frac{2\pi d_i}{\lambda}\cos\theta_i\,/n_i$ and $\frac{\cos\theta_i}{n_i}$, respectively. For TE, we have $q_i = \frac{2\pi d_i}{\lambda} n_i \cos\theta_i$ and $\varsigma_i = n_i \cos\theta_i$.

The total characteristic matrix describing the detector's response to electromagnetic waves is then given by[46, 47]:

$$w_t = W = \begin{pmatrix} W_{11} & W_{12} \\ W_{21} & W_{22} \end{pmatrix} = \prod_{i=1}^{k} w_i$$
$$= (\,W_{pc})^N W_D (W_{pc})^s \quad (5)$$

Wherever, $w_t, w_{pc}, w_D$ are the matrices of the whole structure, the smallest unit in PC of silicon dioxide with silicon, and defect of polystyrene blue layers, respectively.

Equation (5) highlights the characteristic matrix elements that describe the reflectance coefficient of the designed structure [48, 49]:

$$r_1 = \frac{(W_{11}+W_{12}\varsigma_s)2\varsigma_0 - (W_{21}+W_{22}\varsigma_s)}{(W_{11}+W_{12}\varsigma_s)\varsigma_0 + (W_{21}+W_{22}\varsigma_s)} \quad (6)$$

Finally, The reflectivity of the detector is then calculated as[50, 51] :

$$R = |{r_1}^2| \quad (7)$$

## 4. Results

### 4.1. Fitting processing

According to characteristics of polystyrene blue, we will investigate the influence of using it as a defect layer within PCs on detecting on gamma doses. First, we'll present the results of fitting

experimental data to model the refractive index changes under varying gamma doses. From ref[41], we get experimental data which depends on indirect band gap of Ps and its optical energy gap. Meanwhile, fig.3 shows the role of variation in gamma doses and its effect on refractive index of Ps. Thus, the refractive index of Ps blue which labeled by $n_D$ increases toward unirradiation samples until reach. Indeed, $n_D$ alters from 3.81 to 4.67 reached 5 at wavelength 403 nm, when gamma doses vary from 2000 rad until 0 rad or unirradiation.

To simplify, we showcase the fitting treatments applied to the experimental data for the refractive index of polystyrene blue. These treatments show the coincidence between experimental data and fitting results. Equations (8), (9), and (10) represent the fitting degrees for the refractive index data under different gamma doses, with fitting degrees of 8th, 9th, and 8th order, respectively. While Eqs. (8) and (10) share the same fitting degree, Eq. (9) exhibits a higher-order fit with a constant term $u_1$= -4.698204x10$^{-22}$. Also, Table.1 shows the values of constants a, b, c, d, e, f, g, h, and V.

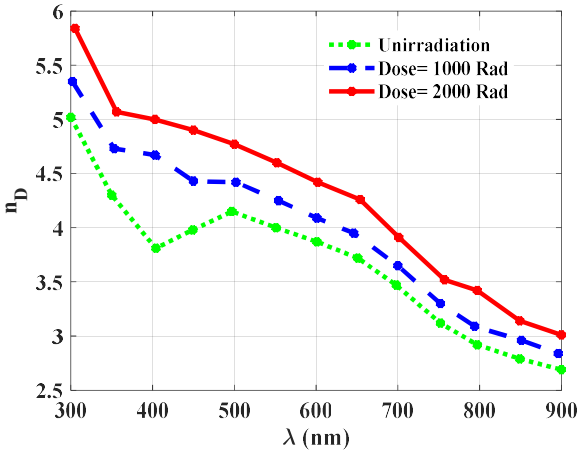


Fig.3: the variation of refractive index of polystrene blue $n_D$ under different doses of irradiation.

Table.1: Numerical constants obtained from the fitting process.

| **Gamma Dose** | **0 Rad** | **1000 Rad** | **2000 Rad** |
|---|---|---|---|
| **Constant a** | $a_0$ =-1.67375892x10$^{-19}$ | $a_1$=2.554456x10$^{-18}$ | $a_2$=7.5495512x10$^{-20}$ |
| **Constant b** | $b_0$=8.11736897x10$^{-16}$ | $b_1$=-6.0980224x10$^{-15}$ | $b_2$=-3.7878843x10$^{-16}$ |
| **Constant c** | $c_0$=-1.69318733x10$^{-12}$ | $c_1$=8.3844449x10$^{-12}$ | $c_2$=8.1869314x10$^{-13}$ |
| **Constant d** | $d_0$=1.98148098x10$^{-09}$ | $d_1$=-7.3131392x10$^{-9}$ | $d_2$=-9.9478905x10$^{-10}$ |
| **Constant e** | $e_0$=-1.42081211x10$^{-6}$ | $e_1$=4.1938866x10$^{-6}$ | $e_2$=7.4277758x10$^{-7}$ |
| **Constant f** | $f_0$= 0.000638096536 | $f_1$=-0.0015804117 | $f_2$=-0.0003488137 |
| **Constant g** | $g_0$=- 0.174938887 | $g_1$=0.3771897 | $g_2$=0.10057325 |
| **Constant h** | $h_0$=26.7106835 | $h_1$=-51.718615 | $h_2$=-16.276603 |
| **Constant V** | $V_0$= -1730.92203 | $V_1$=3108.5254 | $V_2$=1137.3069 |

$$n_D(0\ Rad) = a_0\lambda^8 + b_0\lambda^7 + c_0\lambda^6 + d_0\lambda^5 + e_0\lambda^4 + f_0\lambda^3 + g_0\lambda^2 + h_0\lambda + V_0 \quad (8)$$

$$n_D(1000\ Rad) = u\lambda^9 + a_1\lambda^8 + b_1\lambda^7 + c_1\lambda^6 + d_1\lambda^5 + e_1\lambda^4 + f_1\lambda^3 + g_1\lambda^2 + h_1\lambda + V_1 \quad (9)$$

$$n_D(2000\ Rad) = a_2\lambda^8 + b_2\lambda^7 + c_2\lambda^6 + d_2\lambda^5 + e_2\lambda^4 + f_2\lambda^3 + g_2\lambda^2 + h_2\lambda + V_2 \quad (10)$$

Based on the fitting treatments, we determined the suitable wavelength range for studying the optical properties of PS blue in 1D PCs. This range starts at 300 nm and ended at 600 nm of spectrum.

Furthermore, the presence of the polystyrene (Ps) layer as a defect in the photonic crystals (PCs) also influences the reflectivity (R) and transmittance (T) spectra in the visible range. This defect layer introduces a resonance peak within the photonic band gap (PBG), evident in both R and T spectra. As shown in Fig. 4, the resonance peak occurs at 379.561 nm, with the PBG spanning from 355.39 nm to 426.517 nm.

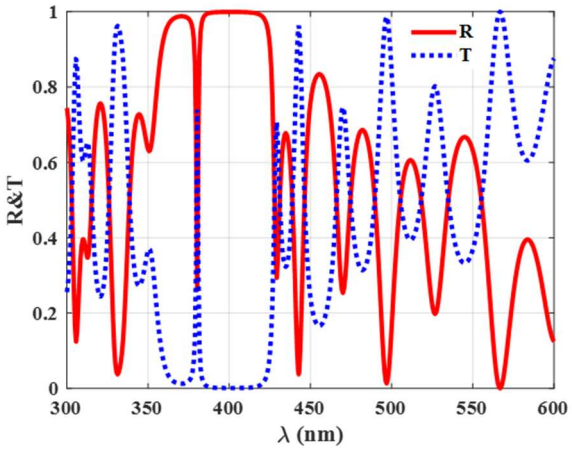


Fig.4: The reflectivity and transmittance spectra of the $[(SiO2/Si)^N/Ps/(SiO2/Si)^s]$ structure regarding the incident wavelengths for a normal incidence case.

### 4.2. Optimization of parameters

Here, as previously mentioned, our structure consists of layer thicknesses d1 = 20 nm, d2 = 85.51 nm, and dD = 20 nm. Under normal incidence, we will examine the optical response of PS blue to low doses of radiation. Subsequently, we will investigate the impact of various factors on the structure's sensitivity under varying irradiation doses, including the influence of layer thickness, incident angle, and periodicity number. Our goal is to optimize sensitivity and other key performance metrics, such as full width at half maximum (FWHM), quality factor (Q), and figure of merit (FOM).

#### 4.2.1. Optimization of thickness

Firstly, We begin by examining, in Fig. 5, how the thickness of the SiO2 layer influences the sensor's performance when exposed to different gamma-ray doses. Fig.5 (a) illustrates the effect of increasing in the thickness of SiO2 layer from 10 nm, 15 nm,20nm, 50 nm, 80 nm,and 150 nm on the sensitivity (S) value. At 1000 rad, the sensitivity values were 0.004833 nm/Rad, 0.006951nm/ Rad, 0.008571nm/Rad, 0.0075nm/Rad, 0.002256nm/Rad, and 0.006381nm/Rad, with corresponding increments in thickness. For a 2000 Rad dose, S values achieved 0.001161, 0.0014565, 0.001713, 0.002472, 0.0012825, and 0.006381 in unit of nm/Rad under the same d1 variation.

Meanwhile, we observed the maximum S in two doses of radiation not agree at the same change in thickness, as shown in Fig.5 (a). Due to the changing in shifting through dip resonance don't compansate the variation in radiation. At 1000 rad, the maximum sensitivity is 0.008571 nm/Rad, occurring at a thickness (d1) of 20 nm. In contrast, at 2000 rad, the maximum sensitivity is 0.002472 nm/Rad, achieved at a thickness of 50 nm. Therfore, we consider another factor to determine the optimal thickness for our design such as the full width at half maximum (FWHM). This factor measures the resonance peak's width at half maximum intensity. Fig.5 (b) clenchs which the optimal thickness of d1 from decreasing in values of FWHM. For both radiation doses, the minimum Full Width at Half Maximum (FWHM) is 0.4, achieved at a thickness (d1) of 50 nm.

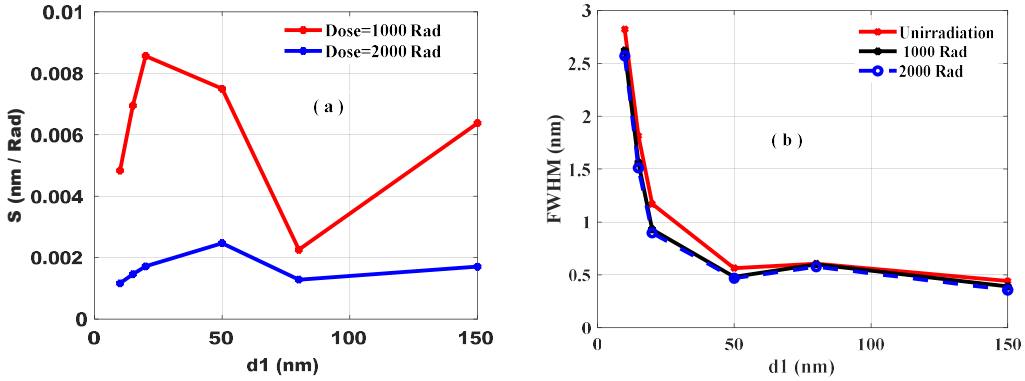


Fig.5: (a) The diagram illustrates the optimal silicon dioxide thickness d1 used to achieve higher sensitivity in our proposed sensor. (b) the effect of variation of d1 on full width at half maximum.

Next, we demonstrate the optimal thickness of the seconed layer d2 of silicon under variation of doses. By increasing the thickness of d2 from 20 nm reache 160 nm, we observed decrement in the S values in both state of doses.This reduction has a significant impact on the behavior of propagating electromagnetic waves and the overall performance of the designed detector.The maximum sensitivities are 0.014643 nm/Rad at 1000 Rad and 0.003307 nm/Rad at 2000 Rad, respectivly. According to two states of radiation dose, the optimal thickness of d2 synchronizes with 25.51 nm ,as represented in Fig.6.

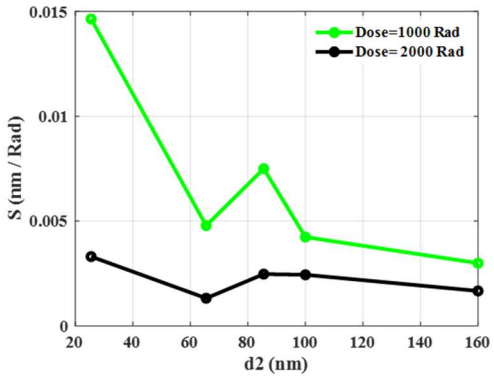


Fig.6: The response of the sensitivity S of the designed sensor versus the thickness of silicon layer $d_2$ at different doses of gamma radiation.

Moreover, Fig.7 illustrates the response of S increment with increasing in the thickness of Ps blue layer. Particularly, the changes in the thickness of this defect provide significant effects on the overall optical properties of the designed structure. However, the polymer defect layer with its

complex dielectric function, gives rise to a resonance peak within the PBG. As previously mentioned, we start by dD equals 20 nm which achieves sensitivity 0.014643 nm/ Rad and 0.003307 nm/ Rad at doses of 1000 and 2000 Rad, respectively. Notably, Fig.7 demonstrated the reduction in dD thickness below 20 nm, also sensitivity drop due to changes in optical path length. Also, the increase in dD over 20 nm led to increments in S values. Therefore, we have now discussed the optimal one of dD through its effect on the S of our detector. Under two conditions of doses, we find both agree with increasing in S at 100 nm and 200 nm of Ps defect layer. However, FWHM gives an indication that the optimal thickness at 100 nm as shown in Fig.7 (b). These sensitivities are 0.02652 nm/ Rad at 1000 Rad and 0.00786 nm/Rad at 2000 Rad.

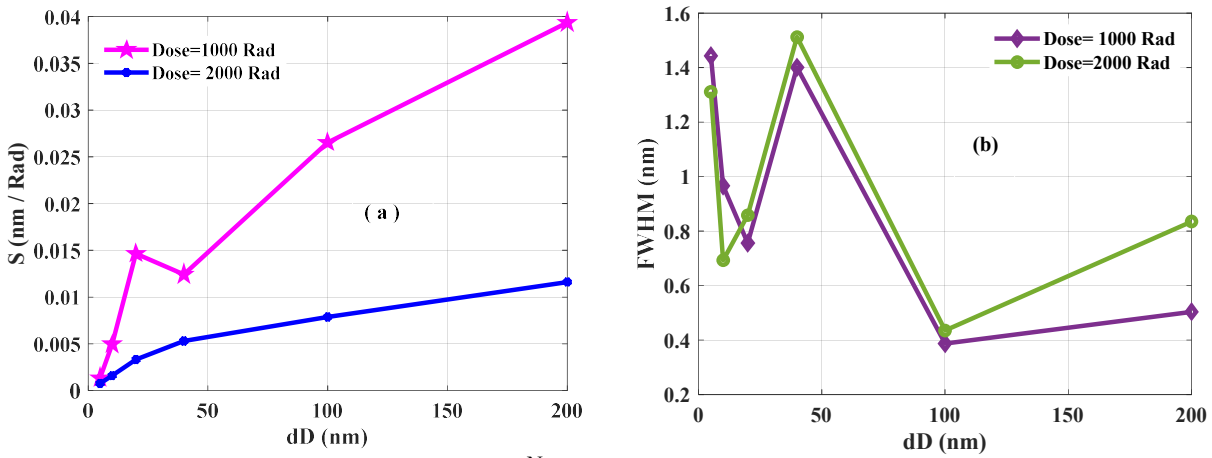


Fig.7: (a) the sensitivity of our $[(SiO2/Si)^{N}/Ps/(SiO2/Si)^{s}]$ detector versus variation in defect of Ps blue thickness under doses of 1000 Rad and 2000 Rad of gamma radiation. (b) the relationship between Full width at half maximum and thickness of defect layer of Ps.

### 4.2.2. Optimization of incident angle

In this subsection, we introduce the role of the angle of incidence on the performance of our detector at the optimum values of d1= 50 nm, d2= 25.51 nm, and dD= 100 nm. The incident angle significantly influences the sensitivity and resonance peak position of the detector. As shown in Fig. 8, varying the incident angle from 0 to 80 degrees for TE polarization results in distinct changes in S values, particularly at low radiation doses. Notably, increasing the incident angle to 80 degrees enhances sensitivity from 0.018842 nm/Rad to 0.028494 nm/Rad. This parameter plays a crucial role in determining the optical path length, similar to the impact of layer thicknesses and incident radiation wavelength. At a dose of 2000 Rad, S exhibits an initial increase from 0.008441nm/Rad with incident angle, reaching its maximum 0.008836 at 80 degrees, to achieve optimal results when doses respond differently to the same factor, an extra parameter is needed to guide the process. As shown in Fig. 8(b), the FWHM factor exhibits a decreasing trend with increasing incident angle for 1000 Rad. For 2000 Rad, the FWHM reaches its minimum value of 0.653 nm at an incident angle of 80 degrees. Thus, the results indicate that an incident angle of 80 degrees provides optimal performance in terms of sensitivity.

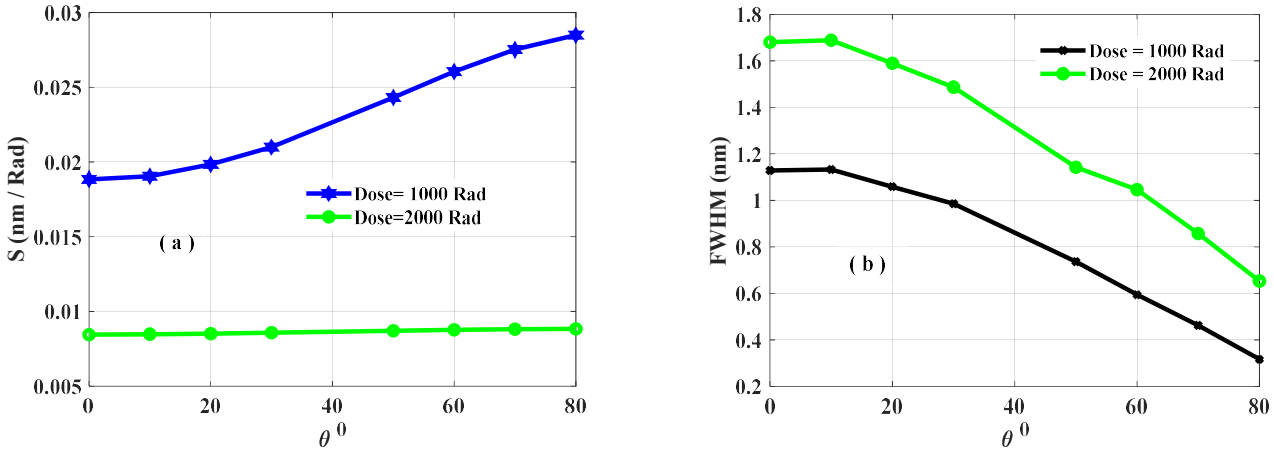


Fig.8: (a) the sensitivity versus the variation of irradiation doses at specific angle of incidence. (b) The variation of the full width at half maximum with respect to irradiation doses is analyzed at specific incident angles.

### 4.2.3. Optimization of periodicity numbers

Based on the optimum values of the previous parameters, we now investigate the optimal value for S regarding periodicity number. In this context, the designed structure has the configuration of $[(SiO_2/Si)^{N=5}/Ps/(SiO_2/Si)^{s=5}]$ including a specific number of periodicities represented in N and s. N represents the number of periodicities ($SiO_2$/Si) before the defect layer (Ps), while s represents the number of periodicities after the defect layer.

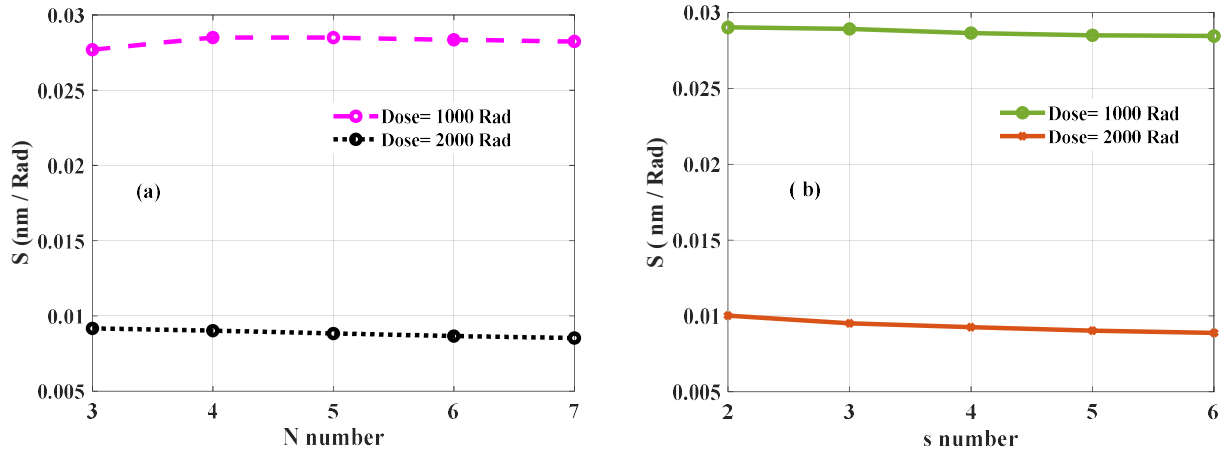


Fig.9: (a) Impact of N on sensitivity before Ps defect layer and (b) impact of s on sensitivity after Ps defect layer at doses of 1000 and 2000 Rad.

For a fixed number of s=5, Fig.9. (a) demonstrates that the best response for the S values over all the considered variation in N number at 4. On the other hand, Fixing N at 4 and decreasing s about 5 increases the S slightly, with a three-decimal-point increment as shown in Fig.9 (b). Furthermore, the optimal sensitivity from two cases number N and s is 0.029017 nm/Rad at 1000 Rad and 0.010008 nm/Rad at 2000 Rad as indicated in Table.2. Thus, the optimal configuration is achieved with N=4 and s=2.

Table.2: illustration the optimal values of N and s numbers of periodicity under doses of 1000 and 2000 Rad.

| Dose (Rad) | N number | S number | Sensitivity S(nm/Rad) |
|---|---|---|---|
| **1000** | **5** | **5** | **0.028494** |
| **2000** | **5** | **5** | **0.008836** |
| **1000** | **4** | **5** | **0.028504** |
| **2000** | **4** | **5** | **0.009019** |
| **1000** | **3** | **5** | **0.027687** |
| **2000** | **3** | **5** | **0.009169** |
| 1000 | **6** | **5** | **0.028351** |
| 2**000** | **6** | **5** | **0.00866** |
| 1**000** | **7** | **5** | **0.028234** |
| 2**000** | **7** | **5** | **0.008528** |
| 1**000** | **4** | **4** | **0.028645** |
| 2000 | **4** | **4** | **0.009254** |
| 1000 | **4** | **3** | **0.028915** |
| 2000 | **4** | **3** | **0.009507** |
| 1000 | **4** | **2** | **0.029017** |
| 2000 | **4** | **2** | **0.010008** |
| 1000 | **4** | **6** | **0.028447** |
| 2000 | **4** | **6** | **0.008871** |

### 4.3. Analysis of detector

Now, the overall performance of the 1D PC sensor is presented, based on optimal geometrical and structural parameters. To sum up, the optimal parameters are summarized as d1=50 nm, d2= 25.51 nm, and dD= 100 nm under angle 80 with number of periodicity N=4, and s=2. Thus, the maximum S reaches 0.029017 nm/Rad at 1000 Rad and 0.010008 nm/Rad at 2000 Rad. As depicted in Fig. (10), we can emphasize the optical properties of the reflectivity spectrum along the direction of incident wavelength. Fig. (10) manifests the emergence of resonance peak under unirradiation sample and this peak due to using defect layer of Ps blue. This resonance peak is located at 446.409 nm of wavelength spectrum. Resonance peak shifts from 446.409 nm to 475.561 nm with 1000 Rad exposure. Moreover, the resonance peak further shifts to 495.333 nm under 2000 Rad, moving toward longer wavelengths.

In what follows, our sensor's efficiency and performance are assessed based on multiple key parameters, including sensitivity, quality factor (Q.F), and figure of merit (FoM), among others. Meanwhile, the sensitivity (S) is defined as the ratio of the change in resonant wavelength ($\Delta\lambda_{res}$) to the change in radiation dose, expressed in nm/Rad such as:

$$S = \frac{\Delta\lambda_{res}}{\Delta\ Dose} \quad (11)$$

Consequently, the sharpness of the resonant peak is reflected by the quality factor and figure of merit, which are inversely related to FWHM, as illustrated in next:

$$Q.F = \frac{\lambda_{res}}{FWHM} \quad (12)$$

$$FoM = \frac{S}{FWHM} \quad (13)$$

$$FWHM = \Delta\lambda_{res} = \Delta(\lambda_L - \lambda_R) \quad (14)$$

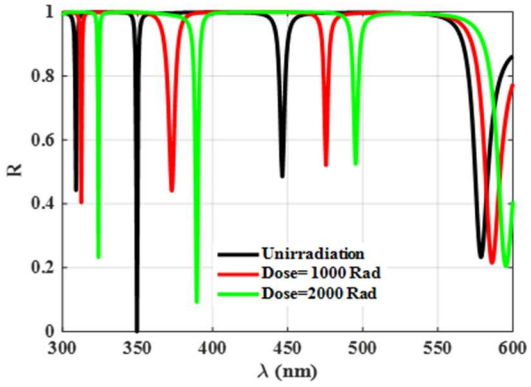


Fig.10: The reflectivity spectra of $[siO_2/Si)^N/Ps/(SiO_2/Si)^s]$ detector regarding the incident wavelengths in absence of gamma radiation and at different values of radiation.

Moreover, key performance factors include Signal-to-Noise Ratio (SnR), Sensor Resolution (SR), Detection Accuracy (D.A), Dynamic Range (D.R), Detection Limit (D.L) which is inversely proportional to the quality factor, and Uncertainty ($U_{peak}$). These parameters can be calculated using specific expressions[52]:

$$SnR = \frac{\Delta\lambda_{res}}{FWHM} \quad (15)$$

$$D.L = \frac{\lambda_{res}}{20\ S\ Q.F} \quad (16)$$

$$SR = (D.L)\ S \quad (17)$$

$$D.A = \frac{1}{FWHM} \quad (18)$$

$$D.R = \frac{\lambda_{res}}{\sqrt{FWHM}} \quad (19)$$

$$U_{Peak} = \frac{2\Delta\lambda_{res}}{9(SnR)^{0.25}} \quad (20)$$

Notably, our detector shows high sensitivity values, especially when detecting low levels of irradiation doses. At 1000 Rad, the Q.F is 171.5592, dropping to 142.5303 when the dose increases to 2000 Rad.

**Conclusion**

In this report, we have described a straightforward and efficient gamma radiation detector based on a one-dimensional photonic crystal structure with a polystyrene blue defect layer. This detector is configured as $[SiO_2/Si)^{N=4}/Ps/(SiO_2/Si)^{s=2}]$. This design facilitates monitoring and quantification of gamma radiation exposure in layers. Moreover, we employed the transfer matrix method to establish a theoretical framework for analyzing numerical results. After optimizing parameters under different doses like thickness, angle of incidence, and periodicity, the detector achieved a sensitivity of 0.029017 nm/Rad and a quality factor of 171.5592 at 1000 Rad. For 2000 Rad, the maximum sensitivity and quality factor are recorded 0.010008 nm/Rad, and 142.5303, respectively. This detector shows promise for applications in food processing industries, particularly for detecting low doses of gamma radiation.

**Acknowledgments**

I would like to extend my sincere gratitude to my supervisor, Zaky. A. Zaky, for his valuable guidance, support, and constructive feedback throughout this project. I am also thankful to the staff at JINR's Frank Laboratory and Neutron Physics for their assistance and encouragement. The JINR Summer Student Program enabled this study by providing a supportive research environment and comprehensive funding, including travel grants, accommodation, and daily stipends.

# References

1. Kajal, R., et al., *Effects of gamma radiation on structural, optical, and electrical properties of SnO2 thin films*. 2023. **15**: p. 100406.
2. Abhirami, K., et al., *Structural, optical and electrical properties of gamma irradiated SnO thin films*. 2013. **91**: p. 35-39.
3. Naikwadi, A.T., et al., *Gamma radiation processed polymeric materials for high performance applications: a review*. 2022. **10**: p. 837111.
4. Chowdhury, S.R. and S.J.J.o.M.C. Sabharwal, *Molecular-scale design of a high performance organic–inorganic hybrid with the help of gamma radiation*. 2011. **21**(19): p. 6999-7006.
5. Sharma, B.K., et al., *Gamma radiation aging of EVA/EPDM blends: Effect of vinyl acetate (VA) content and radiation dose on the alteration in mechanical, thermal, and morphological behavior*. 2018. **135**(18): p. 46216.
6. Zaky, Z.A., et al., *Theoretical study of doped porous silicon in cantor quasi periodic structure for gamma radiation detection*. Scientific Reports, 2025. **15**(1): p. 14995.
7. Zaky, Z.A., et al., *Radiation detector based on coupling between defect mode and topological edge state mode in photonic crystal*. Scientific Reports, 2025. **15**(1): p. 1-14.
8. Zaky, Z.A., et al., *Topological edge state resonance as gamma dosimeter using poly nanocomposite in symmetrical periodic structure*. Scientific Reports, 2025. **15**(1): p. 17753

9. Sayed, F.A., et al., *Quasi periodic photonic crystal as gamma detector using Poly nanocomposite and porous silicon*. Scientific Reports, 2025. **15**(1): p. 18451

10. Zaky, Z.A., et al., *Photonic crystal with a defect layer of silicon containing polymer nanocomposites as radiation detector.* Scientific Reports, 2025. **15**(1): p. 7935.

11. Zaky, Z.A., et al., *Gamma radiation detector using Cantor quasi-periodic photonic crystal based on porous silicon doped with polymer.* International Journal of Modern Physics B, 2024. **38**(30): p. 2450409.

12. Lobez, J.M. and T.M. Swager, *Radiation detection: Resistivity responses in functional poly (olefin sulfone)/carbon nanotube composites.* 2009.

13. Zaky, Z.A., A. Hennache, and V. Zhaketov, *Terahertz metasensor with pseudo parity time symmetry for oral cancer diagnostics*. Scientific Reports, 2025. **15**(1): p. 29424.

14. Zaky A. Zaky, S.A., M. Al-Dossari, D. Mohamed, Vladimir Zhaketov, Arafa H. Aly, *Replacing Toxic Dyes with Photonic Crystals for Printing Applications: Simulation Study*. Applied Optics, 2025. **64**(8).

15. Zaky, Z.A., et al., *Theoretical optimization of Tamm plasmon polariton structure for pressure sensing applications*. Optical and Quantum Electronics, 2023. **55**(8): p. 738.

16. Zaky, Z.A., et al., *Defected photonic crystal as propylene glycol THz sensor using parity-time symmetry.* Scientific Reports, 2024. **14**(1): p. 23209.

17. Zaky, Z.A., et al., *Theoretical analysis of porous silicon one-dimensional photonic crystal doped with magnetized cold plasma for hazardous gases sensing applications*. Optical and Quantum Electronics, 2023. **55**(7): p. 584

18. Zaky, Z.A., et al., *Using Periodic Multilayers of Ferromagnetic and Paramagnetic Layers as Neutron Filter: Simulation Study.* Plasmonics, 2024: p. 1-11.

19. Zaky, Z.A., et al., *Studying the impact of interface roughness on a layered photonic crystal as a sensor.* Physica Scripta, 2023. **98**(10): p. 105527.

20. Wu, C.-J., et al., *Band gap extension in a one-dimensional ternary metal-dielectric photonic crystal.* Progress In Electromagnetics Research, 2010. **102**: p. 81-93.

21. Xu, J., et al., *Layered heterogeneous structures integrated device for multiplication, division arithmetic unit and multiple-physical sensing.* 2024. **36**(9).

22. Segovia-Chaves, F., *Transmittance spectrum of a defective one-dimensional photonic crystal with a protein solution.* Optik, 2021. **231**: p. 166408.

23. Medhat, M., et al., *The Tunability of Tamm Plasmon Resonance Based on the 1D Metamaterials Photonic Crystals for Optical and Sensing Applications*. 2025: p. 1-15.

24. Campbell, M., et al., *Fabrication of photonic crystals for the visible spectrum by holographic lithography.* 2000. **404**(6773): p. 53-56.

25. Lin, S.-y., et al., *A three-dimensional photonic crystal operating at infrared wavelengths*. 1998. **394**(6690): p. 251-253.

26. Kraeh, C., et al., *Fabrication of high aspect ratio microtube arrays for 2D photonic crystals*. 2014. **1**(2): p. 026201.

27. Armstrong, E. and C.J.J.o.m.c.C. O'Dwyer, *Artificial opal photonic crystals and inverse opal structures–fundamentals and applications from optics to energy storage.* 2015. **3**(24): p. 6109-6143.

28. Yoshioka, S. and S.J.P.o.t.R.S.o.L.S.B.B.S. Kinoshita, *Wavelength–selective and anisotropic light–diffusing scale on the wing of the Morpho butterfly.* 2004. **271**(1539): p. 581-587.

29. Zaky, Z.A., et al., *Effective pressure sensor using the parity-time symmetric photonic crystal.* Physica Scripta, 2023. **98**: p. 035522.

30. Zaky, Z.A., et al., *Photonic crystal with magnified resonant peak for biosensing applications.* Physica Scripta, 2023. **98**: p. 055108.

31. Li, Y., et al., *High-contrast infrared polymer photonic crystals fabricated by direct laser writing*. 2018. **43**(19): p. 4711-4714.

32. Yamilov, A., et al., *Ultraviolet Photonic Crystal Laser.* 2004.

33. Wu, C., et al., *High-pressure and high-temperature characteristics of a Fabry–Perot interferometer based on photonic crystal fiber.* Optics letters, 2011. **36**(3): p. 412-414.

34. Karrock, T. and M. Gerken, *Pressure sensor based on flexible photonic crystal membrane.* Biomedical optics express, 2015. **6**(12): p. 4901-4911.

35. Chang, Y.-H., Y.-Y. Jhu, and C.-J. Wu, *Temperature dependence of defect mode in a defective photonic crystal.* Optics Communications, 2012. **285**(6): p. 1501-1504.

36. Singh, A., K.B. Thapa, and N.J.O. Kumar, *Analysis and design of optical biosensors using one-dimensional photonic crystals.* 2015. **126**(2): p. 244-250.

37. Pei, N., et al., *An angle-selective photonic crystal for multi-physical sensing applications*. 2025.

38. Peng, J., et al., *Thin films based one-dimensional photonic crystal for humidity detection.* Sensors and Actuators A: Physical, 2017. **263**: p. 209-215.

39. Elsayed, H.A., F.A. Sayed, and A.H.J.P.S. Aly, *Graphene deposited liquid crystal and thermal sensitivity using photonic crystals.* 2021. **96**(3): p. 035503.

40. Ahmed, A.M. and A. Mehaney, *Ultra-high sensitive 1D porous silicon photonic crystal sensor based on the coupling of Tamm/Fano resonances in the mid-infrared region.* Scientific Reports, 2019. **9**(1): p. 6973.

41. Alwan, T.J.J.T.J.o.P., *Gamma irradiation effect on the optical properties and refractive index dispersion of dye doped polystyrene films.* 2012. **36**(3): p. 377-384.

42. Maebayashi, M., et al., *Study on polystyrene thin film on glass substrate by scanning acoustic microscope.* 2004. **45**(22): p. 7563-7569.

43. Ou, B. and D.J.S.i.C.S.B.C. Li, *Preparation of polystyrene/silica nanocomposites by radical copolymerization of styrene with silica macromonomer*. 2007. **50**(3): p. 385-391.

44. Sabra, W., et al., *Numerical optimization of 1D superconductor photonic crystals pressure sensor for low temperatures applications*. Solid State Communications, 2022. **343**: p. 114671.

45. Sharma, S., et al., *Omnidirectional reflector using linearly graded refractive index profile of 1D binary and ternary photonic crystal*. Optik, 2015. **126**(11-12): p. 1146-1149.

46. Wu, F., et al., *Ultra-large omnidirectional photonic band gaps in one-dimensional ternary photonic crystals composed of plasma, dielectric and hyperbolic metamaterial*. Optical materials, 2021. **111**: p. 110680.

47. Kumar, N., S. Kaliramna, and M. Singh, *Design of cold plasma based ternary photonic crystal for microwave applications*. Silicon, 2021: p. 1-12.

48. Abohassan, K.M., H.S. Ashour, and M.M. Abadla, *A 1D photonic crystal-based sensor for detection of cancerous blood cells*. Optical and Quantum Electronics, 2021. **53**: p. 1-14.

49. Li, Z., et al., *Analysis of photonic band gaps in metamaterial-based one-dimensional ternary photonic crystals*. Indian Journal of Physics, 2019. **93**: p. 511-521.

50. Abadla, M.M., K.M. Abohassan, and H.S. Ashour, *One-dimensional binary photonic crystals of graphene sheets embedded in dielectrics*. Physica B: Condensed Matter, 2021. **601**: p. 412436.

51. Abohassan, K.M., H.S. Ashour, and M.M. Abadla, *One-dimensional ZnSe/ZnS/BK7 ternary planar photonic crystals as wide angle infrared reflectors*. Results in Physics, 2021. **22**: p. 103882.

52. White, I.M. and X. Fan, *On the performance quantification of resonant refractive index sensors*. Optics express, 2008. **16**(2): p. 1020-1028.